Tortuosity in concrete technology – an engineering approach

P. Stroeven

Faculty of Civil Engineering and Geosciences, Delft University of Technology, Delft, the Netherlands

Pore tortuosity is one of the relevant parameters in concrete technology underlying porosimetry. The same holds for crack tortuosity in damage analysis. Hence, this paper concentrates on an engineering approach to obtain geometrical-statistical information on tortuosity. It is stipulated that the model parameters in such analytical methods have old roots. The presented approach as well as comparable data in the international literature point toward an upper limit of tortuosity of 2 for the linear as well as the planar index, so for porosimetry as well as damage analysis on micro-level. Results are depending on magnification in experiments or sensitivity in theoretical approaches. A reduction in magnification finally results in a mono-size, meso-level concept. When pore depercolation is advanced in the cementitious materials, nano-cracking is recognized contributing to porosity and thus to tortuosity. A fractal concept is proposed for modelling this phenomenon yielding enhanced tortuosity in accordance with experimental data in the literature.

1   Introduction

Long-term material behaviour is governed by damage evolution and (polluted) water transport through the pore system, or a combination of both. Damage evolution is based on initially small cracks that are forced to grow and coalesce under loadings, to lead ultimately to an unacceptable state of damage. Damage evolution can also be the result of water transport through the body of the material. The freezing water causes mechanical damage; however, the water can also be polluted thereby gradually destroying the integrity of the material, also involving the reinforcement. Pores are inherent to cementitious materials. They are formed during the hydration process and give rise to a certain level of permeability in the cement paste that is pocketed between the aggregate

grains, and thereby to the concrete as employed in engineering practice. Of course, the degree of permeability depends on the specific combination of technological parameters characterizing the materials on both levels of the microstructure. Further, the degree of water saturation has been shown of crucial importance (Li, *et al.*, 2016; 2017; Kameche, *et al.*, 2014). The pores in cementitious materials form a network structure in which the main channels account for the fluid transport through the material. Hence, the number of such channels, and their size, shape and tortuosity are relevant parameters in that transport process. Yet, herein we will focus on tortuosity.

The cracks form similar spatial network structures under external or internal influences. Researchers in damage mechanics are interested in describing the evolution of the damage structure. Quite some attention has been given in our work to experiments in the direct tension and direct compression domains (Stroeven, 1973; 1979). See also Ringot (1988) for an alternative stereological approach. In fracture mechanics, the internal stress situation is more complicated and the crack structure is therefore significantly schematized (final report of RILEM TC QFS).
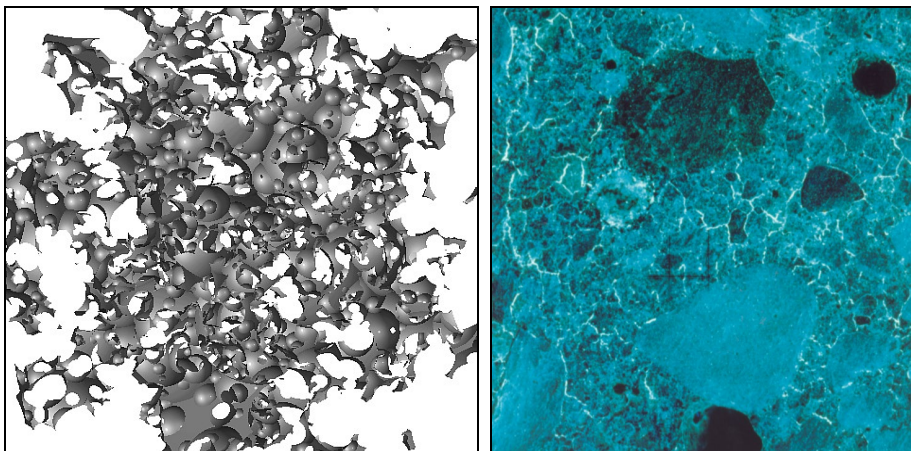

Figure 1. Tortuous and complex 3D pore structure in the vector-based DEM approach to hydrated cement paste after removal of the hydrated particles (Stroeven, M., 1999) (left), and concrete damage in direct compression, visualized in a vertical section. Surface of the specimen's section is sprayed by a fluorescent and photographed under UV light (Stroeven, 1973) (right).
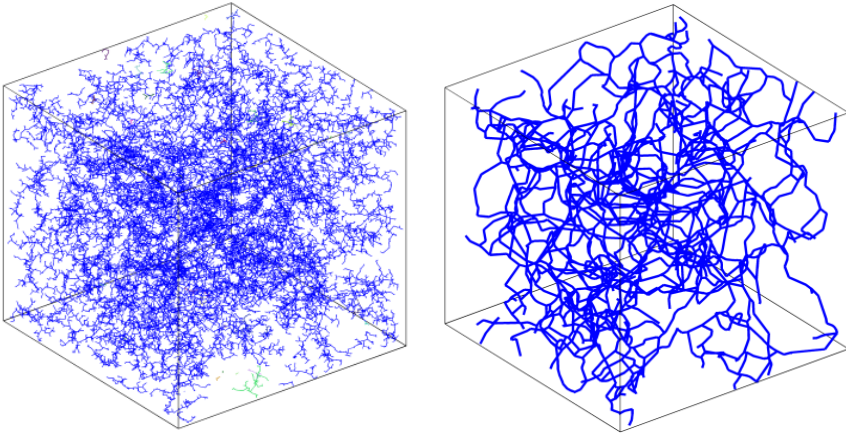
Figure. 2. Double Random Multiple Tree Structuring (DRaMuTS) exploration of virtual cement paste yielded the tree network structure of pores in the case of a specimen with two rigid (left and right) and four permeable surfaces. Pores meander in the 100 μm cube space at 90 days of hydration: w/c = 0.4 and Blaine surface area 300 m²/kg. Porosity is 19%. All detected capillary pores are shown (left)), as well as only the continuous channels connecting the bottom and top surfaces (right) (Stroeven and Li, 2017). Note that 10^5 nodes were distributed in pore space; they form the joints between the straight-line elements building up the pore network skeleton.

Pore tortuosity, as we have used it here, is defined as the ratio of the length of the route of the fluid through a pore channel divided by the straight-line distance between its entrance points on the opposite specimen surfaces. Pore tortuosity assessment offers a linear problem. It has been reported in various studies using different approaches to vary between certain limits (Bathia, 1985; Haughey and Beveridge, 1969; Peterson, 1958; Promentilla, *et al.*, 2009; 2016; Sobiesky, 2016; Sun, *et al.*, 2011; Wong. *et al.*, 2006). In our virtual DEM-based approaches to cementitious systems, information on pore tortuosity can be obtained (Stroeven, *et al.*, 2009; 2012; 2015; Stroeven and Li, 2017; 2018). The bulk of our virtual data on tortuosity is *in statu nascendi* and will be presented in a separate paper with Chinese co-author K. Li, who contributed as PhD student at DUT to the development of the very DEM approach (Li, 2017). Preliminary values of experimental data were found within the range of available data in the literature (indicated later in this publication), and below the herein developed theoretical upper bound value.

Contrary, cracks are planar elements, so will present a planar tortuosity problem. Yet, cracks visualized in sections offer a pattern of lineal elements. In direct tension and

compression cases, sampling will be in sections that are properly adjusted to the loading system. Hence, one section will be oriented in the loading direction and in compression also one perpendicular to it (Stroeven, 1973; 1979). This renders possible a complete analysis of damage characteristics also involving total crack surface area, S, per unit of volume, V, yielding $S/V = S_V$. In the section plane, also linear tortuosity can be assessed, of course.

This paper will concentrate on the modelling of pore and crack structures, so that a concept for tortuosity is obtained. Resulting data will be compared with available data in the literature. The complexity of linear pores and planar cracks in concrete is demonstrated in Figure 1. The pore system developed in hydrating virtual cement paste is revealed at the left after removal of all solid material. At the right is displayed a section of a much larger specimen (some aggregate grains are showing up in grey tones) subjected to uniaxial compression. After spraying with a fluorescent (Stroeven, 1973), the cracks become observable under UV light. At higher magnification, observable crack density is increased, of course. These examples are presented to demonstrate that the tortuosity in both cases needs some simplification. This will be highlighted when the analytical models are developed.

2   Geometrical-statistical approach

First of all, the definition of tortuosity used in this paper (and, generally, throughout concrete technology) should be specified, because different concepts are in use. We have two different cases. In damage analysis we deal with a *planar* phenomenon. Hence, the appropriate 2D definition of tortuosity is the total 2D extent of the damage plane, S_c, divided by the extent of its projection on a plane, A_c, associated with the damage phenomenon (hence parallel with the middle plane). This is illustrated in Figure 3, at the left. The aggregate grains are supposed spherical in the geometrical-statistical treatment of the problem. So, the planar tortuosity index equals $R_s = S_c/A_c$. The damage plane is modelled on *meso-level* as a so-called middle plane from which the particles protrude. Of course, largest part of grains is still embedded, so the smaller part is debonded, as depicted in Figure 3. Hence, the cracks are supposed to follow the middle plane and the surfaces of the aggregate particles protruding from the middle plane.

Additionally, a 1D tortuosity index is needed when confronted with, *e.g.*, pores in concrete. The definition is analogous to the 2D one. Figure 3, at the right, illustrates the simplest approach to the problem. Hence, the length of the line following the middle plane and the surfaces of the aggregate grains, L_p, is divided by the length of its projection on the middle plane, l_p. So, the linear tortuosity index amounts to $R_L = L_p/l_p$. A more appropriate linear concept for porosity, but equally *practical* for porosimetry is only a bit more complicated. Herein, the linear parts of the line do not have to follow a similar direction (they leave the middle plane). Hence, the connecting lines between the particles are composed of smaller straight parts between nodes and can run in arbitrary directions. This is accounted for in the projected length, of course. It is the concept closely simulating the pore distributions derived in the DEM-based simulation set up (Fig. 2), in which a very large number of nodes (10^5) is originally uniformly random (UR) dispersed inside the pores formed in 100 μm cube space.

In Stroeven (2000a,b), the complete geometrical statistical treatment of the problem is developed. For relevant details readers are therefore referred to these publications. In the present paper, we will outline the highlights, making use of these publications, so that we can concentrate more on the engineering interest of users less familiar with (and interested in) geometrical-statistical theory. We will start with the *simplest* model that embodies the notion of cracks going around aggregate grains under loadings, as well as of pores having to traverse around the hydrating cement particles. Figure 3 shows the two simple concepts. Yet, even the selected simple structural concepts will demonstrate the quite complicated type of geometrical-statistical problems that should be solved. In a later stage of treatment of the damage evolution as well as the porosimetry problem, the structural concepts will be modified somewhat (based on the same geometrical-statistical basis) to get closer to actual situations.

An arbitrary *spherical* cap in the fracture surface can be characterized by its height h, which can be at maximum half the diameter ($D/2$) of the very sphere, and the diameter of the intersection circle with the middle plane, x. The latter equals at maximum the diameter of the sphere, D. The surface area of this cap is given in Equation (1).

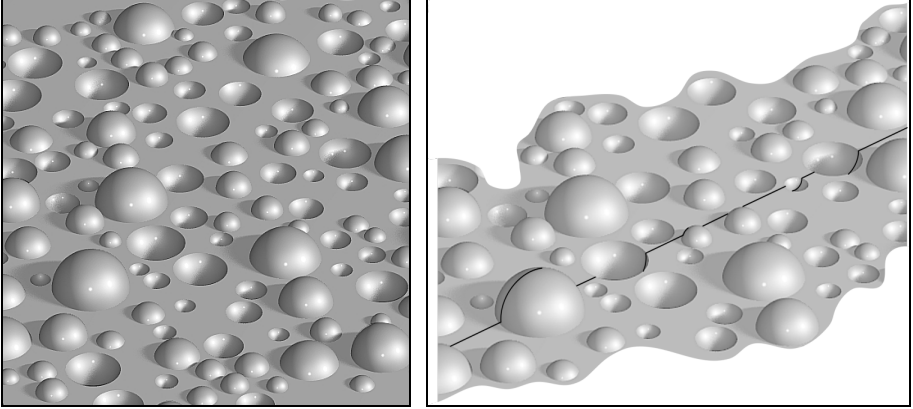$$S = \pi(h^2 + \tfrac{1}{4}x^2) \tag{1}$$

Figure 3. Meso-scale model underlying the planar (left) and linear tortuosity index (right). The cracks, at the left, supposedly circumvent the spherical particles in an UR dispersion of the grains that come in the course of a dividing plane (cracking in concrete due to unidirectional loading). Micro-scale model, at the right, of a pore running through the cementitious matrix and going around the aggregate grains on its way (porosity in concrete).

For mono-size aggregate grains, we see that h fluctuates between 0 and $D/2$ and x between 0 and D. The average value of h is obviously $D/4$, because it is linearly fluctuating. The underlying probabilistic operation is more complicated for x, however, as demonstrated in the publications indicated above. Moreover, we are interested in average morphological characteristics of the fracture surface. So, we have to assess the average surface area in Equation (1), yielding

$$\overline{S} = \pi(\overline{h^2} + \tfrac{1}{4}\overline{x^2}) \tag{2}$$

A bar on top of an expression implies an average. Therefore, determination is required of average values of h^2 and x^2. For cap height h we readily obtain

$$\overline{h} = \frac{2}{D} \int_0^{\pi/2} h \, dh = \frac{D}{4}$$
$$\overline{h^2} = \frac{2}{D} \int_0^{\pi/2} h^2 \, dh = \frac{D^2}{12} \tag{3}$$

Unfortunately, these average values (or moments) for x require considerably more efforts. Readers are therefore referred to the two indicated publications, which delineate the road that can be followed, also for multi-size aggregate concrete. Fortunately, the literature

32

(Kendall and Moran, 1963) presents a direct relationship between the moments of the generation functions of D and x. Here D represents particle size in the mono-size aggregate mixture.

The particle size distribution function (psd) of continuously graded aggregate mixtures in concrete is given by (Stroeven, 1982)

$$f(D) = q \frac{D_o^q}{D^{q+1}} \tag{4}$$

in which D_o stands for minimum grain size in a highly sensitive experimental approach. At a lower sensitivity level, D_o should be associated with *the smallest particle size observed*. The parameter q defines the size distribution curve. As examples, $q = 2.5$ and $q = 3$ yield the so-called Fuller and equal volume fraction curves, respectively.

However, objective was an engineering approach. Hence, we take up again the line of operating for mono-size aggregates. As stipulated earlier, Kendall and Moran (1963) offer a direct way to also assess the moments of x by

$$m_n(x) = M_n(D) \int_0^{\pi/2} (\sin \alpha)^{n+1} \, d\alpha \tag{5}$$

For the mono-size aggregate, Equation (5) yields

$$\bar{x} = m_1(x) = \frac{\pi}{4} M_1(D) = \frac{\pi}{4} D \tag{6}$$

$$\overline{x^2} = m_2(x) = \frac{2}{3} M_2(D) = \frac{2}{3} D^2 \tag{7}$$

Equation (2) yields as a consequence

$$\bar{S} = \pi(\overline{h^2} + \tfrac{1}{4}\overline{x^2}) = \frac{\pi}{4} D^2 \tag{8}$$

The involved cap density in the dividing surface amounts to

$$\frac{N}{A} = N_A = \frac{V_V}{\frac{\pi}{6} D^2} = \frac{6 V_V}{\pi D^2} \tag{9}$$

with N, A and V_V as the number of caps in the middle plane (N), A as the total area (through the intersecting grains) of the middle plane and V_V as the volume fraction of mono-size grains. Finally, the product of Equations (8) and (9) yields the required information; yet, still for mono-size aggregate alone. Hence, we obtain after all those geometrical-statistical manipulations the simple result

$$\overline{S}\,N_A = S_A = \tfrac{3}{2}V_V \tag{10}$$

The last part of the engineering approach is reasoning on the basis of plain logic. Equation (10) holds for all separate fractions in the two different mixes considered. Hence, we finally obtain $S_A = S_{A1} + S_{A2} + \cdots + S_{AN} + = 3\left(V_{V1} + V_{V2} + \cdots + V_{VN}\right)/2$ assuming N fractions in the aggregate mixture. Summarizing, the final result can be formulated as

$$S_A = \tfrac{3}{2}V_V \tag{11}$$

To avoid misunderstandings, the psd in Equation (4) does not represent the grains intersecting the middle plane! Of course, larger grains are more probable to intersect with the middle plane. So, Equation (4) transforms into

$$g(D_c) = \frac{D_c}{\overline{\overline{D}}}\,f(D) \tag{12}$$

where $g(D_c)$ is given for the Fuller and the equal volume fraction mixtures by

$$g(D_c)_{FM} = \frac{D_c}{\overline{D}}\,f(D)_{FM} = \frac{3}{2}\frac{D_o^{1.5}}{D_c^{2.5}} \quad \text{and} \quad g(D_c)_{EV} = \frac{D_c}{\overline{D}}\,f(D)_{EV} = 2\frac{D_o^2}{D_c^3} \tag{13}$$

The required moments of these size distribution functions are readily obtained. For the Fuller distribution we find: $\overline{D}_c = 3D_o$ and $\overline{D_c^2} = 3D_o^{1.5}D_m^{0.5}$. Similarly, for the equal volume fraction distribution: $\overline{D}_c = 2D_o$ and $\overline{D_c^2} = 2D_o^2 \ln(D_m/D_o)$. Herein, D_o and D_m are the smallest (observed) and largest particles in the mixture, respectively. These data can directly be compared with the moments of Equation (4) for appropriate q values demonstrating the relative *roughening* of the fracture surface.

34

3   Tortuosity

Equation (11) brings us very close to the solution for planar tortuosity. We have for the *planar tortuosity index R_S* (with reference to Fig. 3 – at the left)

$$R_S = A_{Am} + S_A = 1 - V_V + \frac{3}{2}V_V = 1 + \frac{1}{2}V_V \tag{14}$$

in which A_{Am} is the area fraction of the middle plane "between" the protruding caps (the matrix portion).

The *linear tortuosity index* follows from the following expression

$$R_1 = 1 - L_L + \frac{\bar{\beta}}{\overline{\sin\beta}} L_L \tag{15}$$

in which $(1 - L_L)$ equals the linear fraction of the line in the middle plane, and L_L equals volume fraction of aggregate particles, V_V. The term $\beta/\sin\beta$ equals the length ratio of curve over the cap and its projected length on the middle plane (Fig. 3 – at the right). These are readily given by

$$\bar{\beta} = \frac{\int_0^{\pi/2} \beta \, d\beta}{\int_0^{\pi/2} d\beta} = \frac{\pi}{4} \quad \text{and} \quad \overline{\sin\beta} = \frac{\int_0^{\pi/2} \sin\beta \, d\beta}{\int_0^{\pi/2} d\beta} = \frac{2}{\pi} \tag{16}$$

Substitution of these results in Equation (15) finally yields

$$R_L = 1 - L_L + \frac{\pi^2}{8}L_L = 1 + (\frac{\pi^2}{8} - 1)L_L \tag{17}$$

with L_L (lineal fraction) = A_A (areal fraction) = V_V (volume fraction).

In the foregoing, the different tortuosity indexes are both derived by geometrical-statistical logic. In practice, it is popular to take the simplest route that starts from the straight-forwardly derived linear tortuosity index and use an available estimate to also obtain the planar tortuosity index. This is also sketched in Stroeven (2000a,b). An interesting concept is that of Coster and Chermant (1987), who proposed

$$R_S \approx \frac{7}{4}R_L - \frac{3}{4} \tag{18}$$

This yields as approximation $R_S = 1 + 0.44\,V_V$, which is not too far off the derived expression in Equation (14). Hence, a practical engineering approach!

4   Improved tortuosity concepts

In fractography, the following improved relationship has been developed for the *planar* tortuosity index (Stroeven, 2000a)

$$R_S = 1 + 2V_V(1 - \frac{3}{4}\omega) \tag{19}$$

in which ω could be interpreted for the present purpose as the fraction of in-plane crack elements of the middle plane only. Hence, the dividing plane is *not flat anymore*, so is transformed into a *dividing surface*; closer to actual situations. For ω = 1 the flat dividing plane as model for cracking is regained. In quantitative damage analysis in the tension-dominated domain the total crack surface area is mostly assumed consisting of two components, a 3D set of IUR distributed cracks and a 2D one in which all cracks are UR distributed parallel to a plane. Alternatively, a two-component mixture of 3D and 1D cracks is used in the compression-dominated domain, whereby the latter cracks are all parallel to an axis. The way to assess the value of ω in experimental settings is extensively discussed in the literature on damage analysis (Stroeven, 1973; 1979).

When cracks coalesce somewhat away from the dividing plane, ω declines. Under strain-controlled conditions, ω will be reduced. When a value of 0.5 is assumed, Equation (19) will yield $R_S = 1 + 5V_V/4$. Hence, for high volume fraction concrete, a planar tortuosity index of about 2 is attained as an upper bound (declining at lower aggregate content). However, here we have to mention again that the experimental approach should be based on the *same sensitivity* as assumed in the theoretical set up. So, cracks should be recorded on the level of minimum grain size. At lower sensitivity, the tortuosity value will decline appropriately. Finally, the mono-size concept is regained at lowest sensitivity level.

As mentioned earlier, the geometric efficiency factor of steel fibre reinforced concrete will offer a relevant improved model for the porosimetry topic. It upgrades the model for linear tortuosity from the 2D one in Figure 3, at the right, into a 3D one. The fibre efficiency is the reversed of the tortuosity index. Figure 4 illustrates this case. The actual fibre dispersion is

36

modelled as a mixture of a 3D IUR component and a 2D one (UR distributed parallel to a plane). We have for the geometric fibre efficiency in a direction in the orientation plane of the 2D fibre portion (Stroeven, 2009; Li and Stroeven, 2020).

$$L_{V\|} = \left(\frac{1}{2} + \left(\frac{2}{\pi} - \frac{1}{2}\right)\omega\right) L_V \qquad (20)$$

in which ω is the total length ratio of the 2D fibre oriented portion over that of the total amount of fibres. $L_{V\|}$ is the total fibre length per unit of volume in the orientation plane of the 2D portion. Since linear tortuosity is given by $L_V / L_{V\|}$, its values range between 2 and $\pi/2$. This is a situation comparable with the linear tortuosity index earlier used for porosimetry, however the latter is more relevant for the porosimetry case. All values mentioned so far are in the range reported in the literature, *i.e.*, √2 (Peterson,1958), √(π/2) (Haughey and Beveridge, 1969) and √3 (Bathia, 1958), these values also referred to by Wong *et al.* (2006), or generally stated as between 1 and 2 (Sun, *et al.*, 2011).
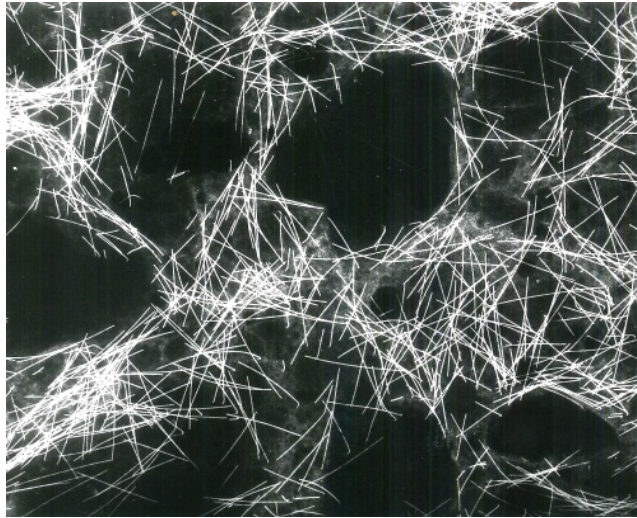

Figure 4. X-ray projection of a slice of steel fibre reinforced concrete. Aggregate grains are "visible" as fibre-free areas. For the present modelling concept, the fibres are supposedly moved by translation and connected at end points yielding a 3D structure resembling the zig-zag shaped pore structure in the DEM-based virtual cement paste as displayed in Figure 2.

5   Discussion

The frequently occurring coefficients in *all* these formulas, *i.e.* 2 and $\pi/2$ (or the reverse), are directly linked up with almost one and a half centuries old Cauchy concepts. For lineal elements we can transform this in the following way. Consider a so called unit sphere (Fig. 5). Herein, the unit sub-lengths, *L*, of all lineal connections between nodes are implanted in such a way that one end point is in the origin, O, of the sphere. In the 2D case of Equations. (1) and (2), the other end points cover uniformly random (UR) the perimeter circle of a plane through O. The average projected length of all lineal connections between nodes amounts therefore

$$\overline{L}' = \frac{\int_0^{\pi/2} \cos\theta\, d\theta}{\int_0^{\pi/2} d\theta} L = \frac{2}{\pi} L \tag{21}$$

This result is obtained for $\omega = 0$ in Equation (20). So, only valid for 2D oriented fibres.

For 3D dispersed node-connecting lines, the end points of the unit sub-length of these lines cover UR the surface area of the unit sphere. The average projected length of *L* along on axis of the sphere is given by

$$\overline{L}' = L \frac{\int_0^{\pi/2}\int_0^{\pi/2} \sin\theta\cos\theta\, d\theta\, d\beta}{\int_0^{\pi/2}\int_0^{\pi/2} d\theta\, d\beta} = \frac{1}{2} L \tag{22}$$

This result is obtained for $\omega = 1$ in Equation (20), so for 3D dispersed fibres only. Hence, it is interesting to note here that a collection of extremely tortuous pores (Fig. 2) connecting opposite surfaces of a concrete specimen are supposedly composed of a *spatial* IUR system of straight short line elements, as argued in the caption of Figures 4 and 5. Average value of their total projections on the respective connecting lines between end points of the individual pores would be precisely twice the average lengths of the connecting lines, according to the Cauchy concept (Cauchy, 1882; Stroeven and Słowik, 2020; Li and Stroeven, 2020). Since one can expect a portion of line elements in the direction of the connecting line (other than contained in the IUR system), the factor of 2 can be considered an upper bound. Of course, pore depercolation due to prolonged hardening will lead to increasing tortuosity. This upper bound value and the effect of hydration are also reported

38

by Promentilla, *et al*. (2009; 2016). The approach is realistic for the *hardened cement paste* investigated in virtual reality. These pockets of hardened cement are located between aggregate grains in the actual concrete. The tortuosity inside the cement paste pockets can be expected the dominating feature in concrete, too, also seeing the relatively small value of tortuosity predicted by Equation (17) for relevant volume fractions of grains. Just a minor enhancement could be expected.

But at further declining porosity, when pore depercolation is advanced, pores should additionally be considered that make on *nano-level* additional detours through so far considered crack free material. This transforms the concept into a *quasi-fractal system* (Stroeven, 1991; 1992). In the high-density hydrate structure, these pores can still contribute to porosity and so to tortuosity. A fractal concept could be employed in the porosity case of the concept underlying Equation (17). However, also in fractography this is a relevant development. Hence, we have selected Equation (19) for demonstration purposes

$$\log\left(1+2V_V(M)(1-\tfrac{3}{4}\omega)\right)=(D-1)\log M+C \tag{23}$$
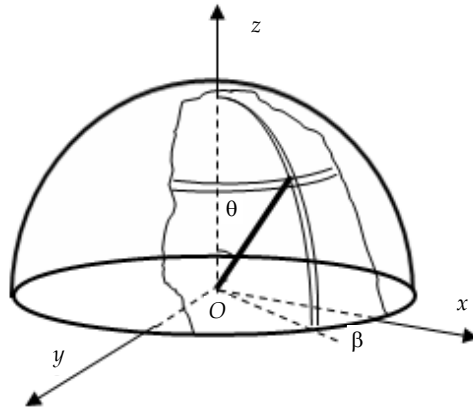

Figure 5. Visualization by sphere model of orientation distribution of mono-size fibre elements in SFRC specimen (Fig. 4). Fibre elements are considered translated from bulk to join in one of their ends in point O. As a consequence, other ends will UR cover the surface of the sphere with unit radius, L. In the present case, fibres are replaced by approximately linear elements of the pore system. In the earlier mentioned DEM-based virtual cement paste, the pores are sampled by such straight-line elements that are the result of infinitely small robots moving along pore length in a slightly zig-zag course (Stroeven, et al., 2012; Stroeven and Li, 2017).

with D as fractal dimension and M as magnification (so, reflecting *sensitivity*). We have recorded D values between 1.10 and 1.13, close to experimental data published by El-Saouma (1990). In Stroeven (1992) this operation is performed on the linear roughness index, revealing for the two mentioned psd's slightly curved lines in the loglog plot of R_L versus M. This can equally be realized for Equation (23) demonstrating R_S to be depending on sensitivity of the approach. However, the underlying *geometrical* concept of interpretation in the current case may start with Koch's snowflake (McWorter and Tazelaar, 1987) with $D = 1.26$. However, the idea can also be used for cracking or porosity in concrete visualized on a high level of magnification. The four mono-size straight lines of the snowflake have three nodes as joints. The outer lines run in the same direction and the couple in the middle forms a mountain peak. The idea is that at increasing magnification, the same mountain peak concept is superimposed on all line elements, thereby increasing tortuosity. This can again be accomplished for still increasing magnifications.

For that purpose, we can use the Cauchy solutions in a more intuitive approach. In the case of the linear tortuosity index, we start with at nodes connected line elements that are approximately 3D (IUR) dispersed between end points in the outer surfaces of the specimen. This is the fibre dispersion concept illustrated in Figure 4. For that case, we have seen that the planar tortuosity index should be at most 2. Suppose now that at a more advanced depercolation state, say at $p = 0.2\sim2.5$, detours are formed in a large number of locations in the main pore channels. When globally speaking, we can treat them as spherical, the average contribution on this higher magnification level to tortuosity will be at most 2 again. Hence, the tortuosity plateau at 2 for low density cases (say, at $p = 0.4$) will start to rise to a value of 4 (at, say, $p = 0.25$). At higher magnification this process may continue in a similar fashion until the pore depercolation process is completed leading to an additional increase of tortuosity by a factor of 2. We see this behavior reflected in a publication of Promentilla, *et al.* (2009), in which indeed the tortuosity level of 2 at $p \sim 0.4$ starts to bend upward terminating at a level of about 8 at very high material density.

A final note on the virtual cement paste to which we referred a number of times. Details can be found in papers referred at. Yet, for the interested reader just a number of characteristics that make the link more obvious with quantitative porosimetry, in the present case to assess tortuosity. The spherical cement particles are distributed by well-known discrete element method (Stroeven and Li, 2017; 2018) and thereupon hydrated

with an upgraded concept of IPKM (Navi and Pignat, 1996; Le, *et al.*, 2013). The pores visualized in Figure 2 are delineated by DRaMuTS, which is an upgraded robotics concept of LaValle and Kuffner (2001). Pore size is obtained by star probing (Stroeven, 2019), a method used in life science experimental settings. A traditional pore network analysis is finally performed on a somewhat simplified pore network. Specifically, the lineal pore elements between nodes are schematizes as cylinders (Le, *et al.*, 2013). This renders possible estimating the flow through the pore network structure. However, this is valid only for fully saturated concrete. For *practical situations* of partly saturated concrete, we have designed obstruction objects in pores, simulating the effect of water in the pores (Li and Stroeven, 2016; 2017; Kameche, *et al.*, 2014).

6   Conclusions

This paper presents an engineering approach to tortuosity that is a major parameter in spatial models of damage and porosity in concrete. The geometrical-statistical background for deriving the linear and planar tortuosity index, R_L and R_S , respectively, is discussed. Since the derivation of the planar index goes deeper into this for concrete technologists quite alien piece of science, an approximate assessment is available in the international literature, and thus also presented herein. The underlying geometrical concept may be considered in some cases too simple. Therefore, the steel fibre dispersion analog is advocated, yielding an improved expression for the linear tortuosity index. For damage assessment also a somewhat improved concept is presented, whereby the original flatness of the middle plane is cancelled. Hence, in direct tension or compression tests, the major part of damage evolution may be assumed consisting of 2D cracks, in accordance with the original set up constituting a flat middle plane and running around the aggregate grains intersecting with the middle plane. The improvement consists of adding an IUR system of, so called, 3D cracks.

It is stressed that all constants in such models were originally derived by Cauchy, almost 1.5 century ago. The above-mentioned improved concepts for linear and planar tortuosity point to an upper bound value of 2. Some results available in the international literature are mentioned, revealing a range of values with 2 as upper bound. Advanced testing for porosity at low porosity values (so very advanced depercolation) have revealed higher values that can be explained by nano-cracking in experiments and a fractal concept in modelling.

41

References

Bathia, S.K. (1985). Directional autocorrelation and diffusional tortuosity of capillary porous media. *J. Catalysis*, **93**:192-196.

Cauchy, A. (1882). *Mémoires sur la rectification des courbes et la quadrature des surfaces courbes*. Cambridge Univ. Press, Cambridge, UK (in French)

Coster, M., Chermant, J-L. (1983). Recent developments in quantitative fractography. *Int. Met Rev.*, **28**:228-250

El-Saouma, V.E., Barton, C.C., Gamaleldin, N.A. (1990). Fractal characterization of fracture surfaces in concrete. *Engr. Fract. Mech.*, **35**:47-53

Haughey, D.P., Beveridge, G.S.G. (1969). Structural properties of patched beds. *Can. J. Chem. Eng.*, **47**:130-140.

He, L.B.N. (2015). *Micro-porosimetry of virtual cementitious materials. Structural impact on mechanical and durability evolution*. PhD Thesis, Delft Univ. Techn., Delft.

Kameche, Z.A., Ghomari, F., Choinska, M. Khelidj. A. (2014). Assessment of liquid water and gas permeabilities of partially saturated ordinary concrete, *Constr. Build. Mater.*, **65**: 551-565.

LaValle, S.M., Kuffner J.J. (2001). Randomized kynodynamic planning. *Int. J. Robot. Res.*, **20**(5):378-400

Kendall, M.G., Moran, P.A.P. (1963). *Geometric probability*, London, C. Griffin Co.

Le, L.B.N., Stroeven, M., Sluys, L.J., Stroeven, P. (2013). A novel numerical multi-component model for simulating hydration of cement. *Comp. Mat. Sci.*, **78**:12-21

Li, K. (2017). *Numerical determination of permeability in unsaturated cementitious materials*. PhD Thesis, Delft Univ. Techn., Gildeprint.

Li, K., Stroeven, M., Stroeven, P., Sluys, L.J. (2017). Effects of technological parameters on permeability estimation of partially saturated cement paste by DEM approach. *Cem. Concr. Comp.*, **84**:222-231

Li, K., Stroeven, M., Stroeven, P., Sluys, L.J. (2016). Investigation of liquid water and gas permeability of partially saturated cement paste by DEM approach. *Cem, Concr. Res.*, **83**:104-113

Li, K., Stroeven, P. (2020). Bridging the gap between structural levels in concrete technology – principles of geometric averaging. *Mat. Today Comm.*, **24**:1-8

McWorter, W.A. Jr., Tazelaar, J.M. (1987), Creating fractals. *Byte*, August 1987, pp. 123-134

Navi, P., Pignat, C. (1996). Simulation of cement hydration and connectivity of the capillary pore space. *Adv. Cem. Bas. Mat.*, **4**:58-67

Peterson, E.E. (1958). Diffusion in a pore of varying cross section. *Am. Inst. Chem. Eng.*, **4**:343-345

Promentilla, M.A.B., Sugiyama, T., Hitomi, T., Takeda, N. (2009). Quantification of tortuosity in hardened cement pastes using synchrotron-based X-ray computed microtomography. *Cem. Concr. Res.*, **39**(6): 548-557

Promentilla, M.A.B., Cortez, S.M., Papel, R.A.D.C, Tablada, B.M., Sugiyama, T. (2016). Evaluation of microstructure and transport properties of deteriorated cementitious materials from their X-ray computed tomography (CT) images. *Mats.* **9**(5), 388 (doi:10.3390/ma9050388)

Ringot, E. (1988). Automatic quantification of microcracks network by stereological method of total projections in concrete. *Cem. Concr. Res.*, **18**:35-43

Sobieski, W. (2016). The use of Path Tracking Method for determining the tortuosity field in a porous bed. *Gran. Mats.*, **18**(72):9 pages

Stroeven, M. (1999). *Discrete numerical modelling of composite materials. Application to cementitious materials*. PhD Thesis, Delft Univ. Techn. Meinema, Delft.

Stroeven, P. (1973). *Some aspects of the micromechanics of concrete*. PhD Thesis Delft Univ. Techn., Delft

Stroeven, P. (1979). Geometric probability approach to the examination of microcracking in plain concrete. *J. Mat. Sci.*, **14**:1141-1151

Stroeven, P. (1982). Structural modelling of plain and fiber-reinforced concrete; a morphological approach to a cracked region. *Comp.*, **13**:129-139

Stroeven, P. (1991). Fractal aspects of damage in concrete. In: *Brittle Matrix Composites 3* (Brandt AM, Marshall IH, eds), Elsevier, Warsaw. pp.1-10.

Stroeven, P. (1992). Fractal aspects and fractography in concrete technology. *Acta Stereol.*, **11**(suppl.1):321-326

Stroeven, P. (2000a). A stereological approach to roughness of fracture surfaces and tortuosity of transport paths in concrete. *Cem. Concr. Comp.*, **22**:331-341

Stroeven, P. (2000b). Stereological estimates for roughness and tortuosity in cementitious composites. *Im. Anal. Stereol.*, **19**:67-70

Stroeven, P. (2009). Stereological principles of spatial modeling applied to steel fiber-reinforced concrete in tension. *ACI Mat. J.*, **106**(3):1-11

Stroeven, P. (2019), Probing pores by stars – An essential module in porosimetry and permeability estimation methodology of virtual cement paste. *Heron*, **3**:265-295

Stroeven, P., Słowik, M. (2020). Cauchy-based modelling in cementitious materials technology. *Arch. Civ. Engn.*, Vol **LXVI**(2):179-190

Stroeven, P., Hu, J., Stroeven, M. (2009). On the usefulness of discrete element modelling of particle packing for material characterization in concrete technology. *Comp. Concr.*, **6**:133-153

Stroeven, P., Le, L.B.N., Sluys, L.J., He, H. (2012). Porosimetry by double random multiple tree structuring. *Im. Anal. Stereol.*, **31**: 55-63.

Stroeven, P., Li, K., Le, L.B.N., He, H., Stroeven, M. (2015). Capabilities for property assessment on different levels of the microstructure of DEM-simulated cementitious materials. *Constr. Build. Mat.*, **88**:105-117

Stroeven, P., Li, K. (2017). A modern approach to porosimetry of virtual cementitious materials, *Mag. Concr. Res.*, **69**(23):1212-1217

Stroeven, P., Li, K.,. (2018). R.S.A. vs D.E.M. in view of particle packing-related properties of cementitious materials, *Comp. Concr.*, **22**(1):83-91

Sun, G-W., Sun, W., Zhang, Y-S., Liu, Z-Y. (2011). Relationship between chloride diffusivity and pore structure of hardened cement paste. *J. Zhejiang Univ. Sci. A.*, **12**(5):360-367.

Wong, H.S., Buenfeld, N.R., Head, M.K. (2006). Estimating transport properties of mortars using image analysis on backscattered electron images. *Cem. Concr. Res.*, **36**(8):1556-1566.